Fully Fabric High Impedance Surface-Enabled Antenna for Wearable Medical Applications

ADEL Y. I. ASHYAP[1], **SAMSUL HAIMI BIN DAHLAN**[1],
ZUHAIRIAH ZAINAL ABIDIN[2], (Member, IEEE),
SHARUL KAMAL ABDUL RAHIM[3], (Senior Member, IEEE),
HUDA A. MAJID[1], (Member, IEEE),
ABDULRAHMAN S. M. ALQADAMI[4], (Graduate Student Member, IEEE),
AND MOHAMED EL ATRASH[5], (Student Member, IEEE)

[1]Center for Applied Electromagnetic (EMCenter), Faculty of Electrical and Electronic Engineering, Universiti Tun Hussein Onn Malaysia (UTHM), Batu Pahat 86400, Malaysia
[2]Advanced Telecommunication Research Center (ATRC), Faculty of Electrical and Electronic Engineering, Universiti Tun Hussein Onn Malaysia (UTHM), Batu Pahat 86400, Malaysia
[3]Wireless Communication Centre (WCC), Faculty of Engineering, Universiti Teknologi Malaysia (UTM), Skudai 81310, Malaysia
[4]School of Information Technology and Electrical Engineering (ITEE), The University of Queensland, Brisbane, QLD 4072, Australia
[5]Department of Electrical Communication and Electronics Systems Engineering (ECE), October University for Modern Sciences and Arts, Cairo 12451, Egypt

Corresponding authors: Samsul Haimi Bin Dahlan (samsulh@uthm.edu.my) and Zuhairiah Zainal Abidin (zuhairia@uthm.edu.my)

ABSTRACT The compact and robust high-impedance surface (HIS) integrated with the antenna is designed to operate at a frequency of 2.45 GHz for wearable applications. They are made of highly flexible fabric material. The overall size is $45 \times 45 \times 2.4$ mm^3 which equivalent to $0.37\lambda o \times 0.37\lambda o \times 0.02$ mm^3. The value of using HIS lies in protecting the human body from harmful radiation and maintaining the performance of the antenna, which may be affected by the high conductivity of the human body. Besides, setting the antenna on the human body by itself detunes the frequency, but by adding HIS, it becomes robust and efficient for body loading and deformation. Integrated antenna with HIS demonstrates excellent performance, such as a gain of 7.47 dBi, efficiency of 71.8% and FBR of 10.8 dB. It also reduces the SAR below safety limits. The reduction is more than 95%. Therefore, the presented design was considered suitable for wearable applications. Further study was also performed to show the useful of placing antenna over HIS compared to the use of perfect electric conductor (PEC). The integrated design was also investigated with the worst case of varying the permittivity of body equivalent model which shows excellent performance in term of reflection coefficient and SAR levels. Hence, the integrated antenna with HIS is mechanically robust to human body tissue loading, and it is highly appropriate for body-worn applications.

INDEX TERMS HIS, AMC, EBG, warble antenna, SAR.

I. INTRODUCTION

Recently, a wireless body area network (WBAN) devices have been used extensively in a variety of fields, such as health care, emergency rescue services, remote monitoring, military warfare, wearable computing, entertainment, and sports. These applications allowed WBAN to receive considerable attention from many academics, industrialists and researchers [1]–[3]. Wearable antennas play an essential role in the WBAN and have received considerable research attention. As wearable antennas operate close to the body, their performance is degraded compared to free space, such as efficiency, gain, and resonant frequency. This is due to the strong coupling with the body, which are lossy and non-homogeneous material [4]–[6]. Besides, the impact of wearable antennas on tissues characterized by a specific absorption rate (SAR) should be considered to ensure that there is no effect on tissues and that their values are reduced to meet the safety level [7]. The design of the wearable antenna was, therefore considered a challenging task.

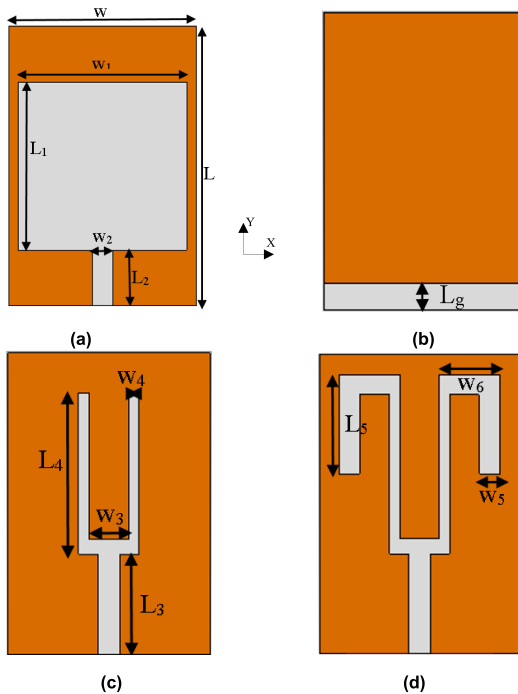The associate editor coordinating the review of this manuscript and approving it for publication was Chinmoy Saha.

FIGURE 1. Evolution of proposed design (a) CMPA, (b) Ground plane, (c) U-shaped antenna, and (d) Proposed antenna.

Various types of flexible/wearable antenna configurations have been proposed and studied in previous years, such as fractal-based patch antennas [8], microstrip patch antennas [9], flat F-shaped antenna [10], PIFA antenna [11], vertical planar monopoles [12], and cavity-backed antennas [13]. These configurations suffer from several drawbacks: greater size, thicker, narrow bandwidth, and high back radiation. They also had limitations to be applied to flexible/wearable devices. Thus, high impedance surface (HIS) structures are introduced in the design of wearable antennas to provide isolation between the body and the antenna and to allow the SAR levels to comply with the safety limits set by the FCC. On the other hand, these structures still have some disadvantages that remain unresolved, such as low front to back ratio (FBR) [14]–[17], designed on semi-flexible substrate that cannot stand for several degrees of bending [18], [19], and electrically large or thick for wearable devices [20]–[32].

This research paper presents a low-profile, compact, conformal, wearable fabric antenna with HIS for wearable applications. The addition of HIS to the wearable antenna design is worthy of its artificially unique feature, mimicking the functionality of a perfect magnetic conductor (PMC) that does not exist in nature [33]. Besides, they are capable of controlling electromagnetic behaviors. As a result, the performance of wearable antennas has significantly improved efficiency, FBR, directivity and reduced SAR value.

II. ANTENNA PERFORMANCE IN FREE SPACE AND ON BODY

A jeans substrate with a dielectric constant of 1.7 mm and a thickness of 0.7 mm is used as an antenna support material.
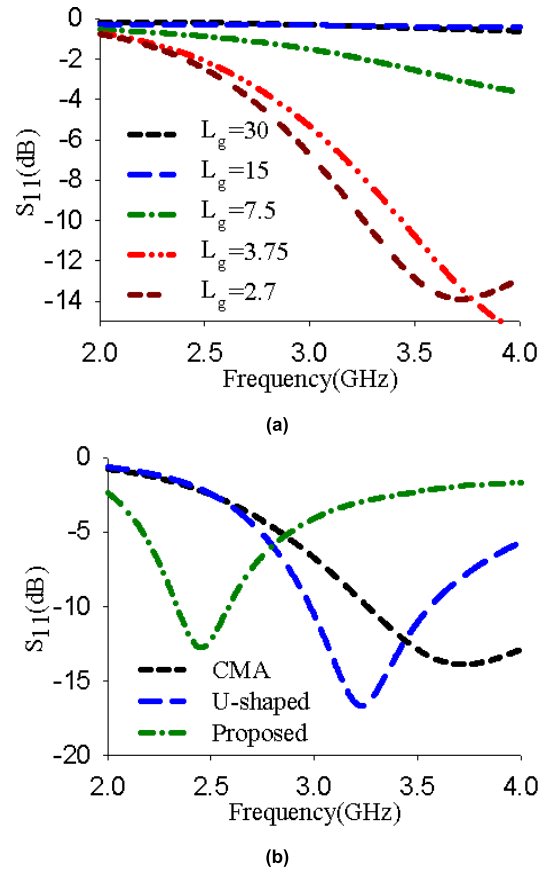

FIGURE 2. Scattering parameter (a) Varying the length of the ground of CMPA, and (b) Comparisons between CMPA, U-shaped antenna and proposed antenna.

Whereas a Shieldit^{TM} with a thickness of 0.17 mm used as a conductive layer. The evolution of the proposed design is based on the Conventional Microstrip Patch Antenna (CMPA), as shown in Fig.1 (a). The dielectric dimension is chosen to be $30 \times 20 \times 0.7$ mm^3 ($0.25 \lambda o \times 0.16 \lambda o \times 0.006 \lambda o$ mm^3), which can be adapted to the growth of wearable devices. Fig.2 (a) shows the S_{11} of the CMPA with full ground (Lg = 30). The result demonstrate that the CMPA does not operate with the full ground plane. We, therefore, conducted a parametric study on the effect of the ground plane on the CMPA. The length ranged from 30 mm to 2.7 mm, where a resonant frequency was observed. However, the CMPA still resonates at 3.7 GHz. To further shift the resonant frequency, a slot is introduced in the CMPA to form U-shaped, as shown in Fig.1(c). The slot helps to divert the current path; as a result, the resonant frequency shifted to the lower band at 3.2 GHz, as shown in Fig.2 (b). The inverted L-shaped was then added to the two arms of the U-shaped to form the final design, as illustrated in Fig.1 (d). The proposed design shows a resonant frequency of 2.45 GHz at the desired band. This shaped combination helps to maintain the desired band with a small antenna size. The optimal dimensions of the evaluation process are shown in Table 1.

For better understanding, the surface current of the evaluated designs is carried out, as shown in Fig.3.
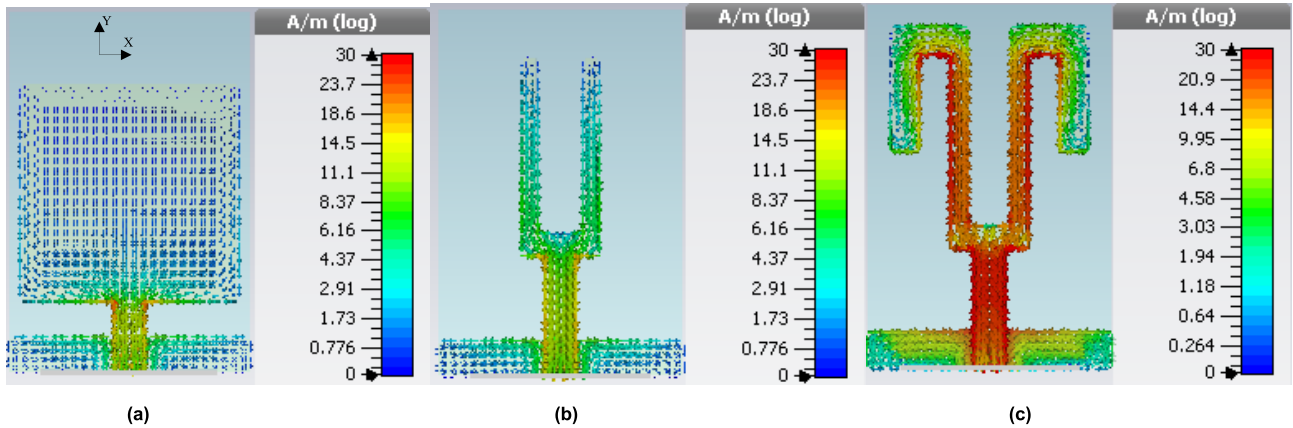
FIGURE 3. Surface current (a) CMPA, (b) U-shaped antenna, (c) Proposed design.

TABLE 1. Optimal values of the evolution antenna dimensions (mm).

Parameter	w	w_1	w_2	w_3	w_4	w_5	w_6
Value	20	18	2.146	4	1	2	6
Parameter	L	L_1	L_2	L_3	L_4	L_5	L_g
Value	30	18	6	10	16	10	2.7

The simulations are performed at the resonant frequency 2.45 GHz for the CMPA, U-shaped and proposed design. It is observed that the current distribution is less for the case of CMPA and U-shaped while highly concentrated for the case of the proposed design. This indicates that the combination of the U-shaped with inverted L-shaped divert the current and increase its path which shift the resonant frequency from higher to lower band.

Since the application of the design is for wearable use, its output must be examined when mounted on the human body. The presented antenna was placed directly on the phantom models as shown in Fig.4 (a). The simulated S_{11} is shown in Fig.4 (b) in free space and on the body. The loading of the antenna on the body caused the frequency of the resonance to detune compared to free space. This is due to the body is hugely conductive in contrast with the antenna substrate. Therefore, the HIS structure is presented in this paper to overcome this problem. HIS helps to isolate the antenna from the body, the SAR level to meet the specifications and enhance the efficiency of the antenna.

III. HIS DESIGN
On the same supporting material as the antenna, the HIS structure is printed. The HIS characteristics are analyzed using a suspended line approach [34]. The HIS structures are placed in between the ground plane and the suspended line forming a sandwich-like shape as reveals Fig.5.

The arrangement includes 3×3 cells of the unit. In order to cover the desired band, few steps had been carried out. Firstly, the unit cell initially formed from a square patch of 44.667×44.667 mm^2 that formed an array of
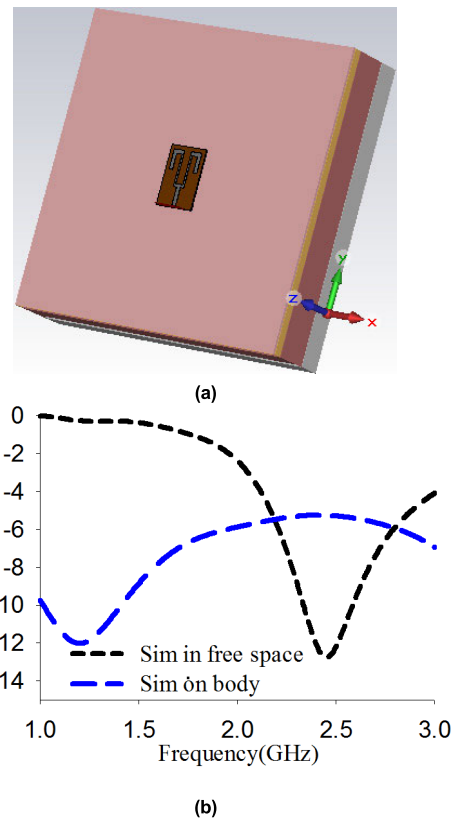

FIGURE 4. (a) Antenna on phantoms model, and (b) Performance of the proposed antenna in free space and on body.

134×134 mm^2. Then, a horizontal square slot is inserted in the middle of the square patch to minimize the size of the unit cell to 30×30 mm^2, resulting in an array size of 90×90 mm^2 with a decrease of 54.89 % compared to the conventional square patch. Finally, two vertical slots are inserted at the end of the square slot to form an I-shaped slot that reduced the size of the unit cell to 15×15 mm^2 which formed an array of 45×45 mm^2 with a reduction of 88.72% compared to the conventional square slot. Fig. 6 depicts the HIS evolution process. The inclusion of slots on the radiating element modifies the
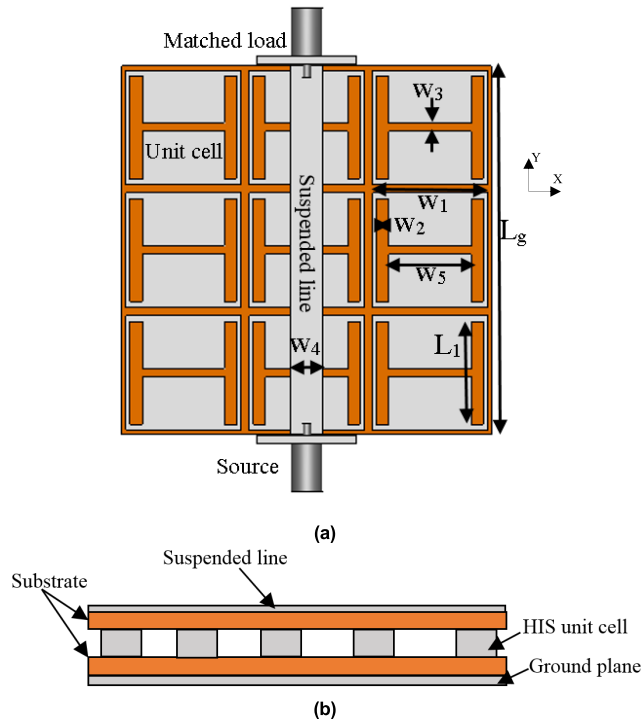
(a)

(b)

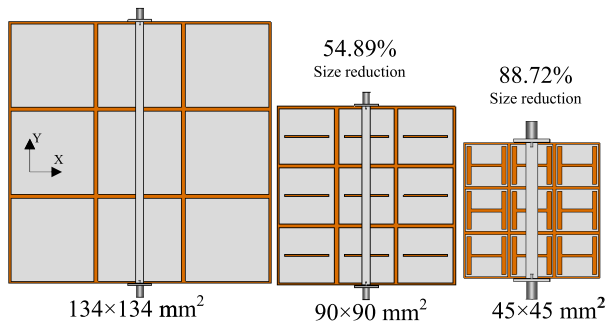**FIGURE 5.** Suspended line method (a) top view, (b) Side view.

FIGURE 6. Evolution process of 3 × 3 HIS with the percentage size reduction (a) square patch, (b) square patch with horizontal square slot, and (c) square patch with I-shaped slot.

current distribution and increases the sufficient current path length. The resonance frequency is also decreased, which leads to a reduction in the size of the HIS. The bandwidth was also improved compared to the traditional square patch due to the lower Q factor [35]. The total size of the final design is $45 \times 45 \times 0.7$ mm^3 ($0.37\lambda o \times 0.37\lambda o \times 0.006$ mm^3), which is compact compared to the structures previously described in [7], [13], [14]– [32].

Fig. 7 presents the S-parameters of the evolution process of HIS. By adding the slot, the bandwidth is improved because of a lower Q factor [35]. The final presented design shows a bandwidth of −10 dB between 1.38 GHz and 2.73 GHz. The HIS also can suppress the antenna's surface wave in its frequency band to enhance efficiency and effectiveness. Table 2 indicates the optimal dimensions of HIS.
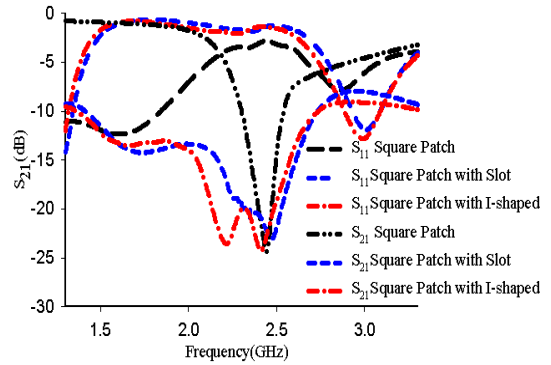

FIGURE 7. Characteristics of HIS.

TABLE 2. Optimal values of the HIS dimensions (mm).

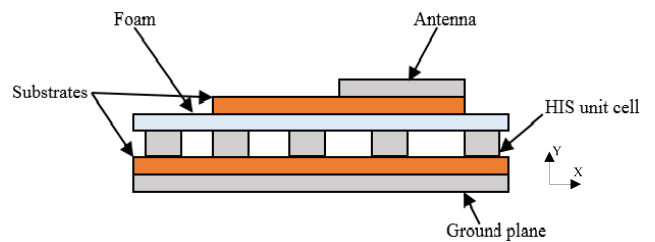| Parameter	L_g	L_1	w_1	w_2	w_3	w_4	w_5
Value	45	12.6	14	1.5	1	4	10.04

FIGURE 8. Prototype of the integrated antenna with HIS.

IV. ANTENNA WITH HIS PERFORMANCE IN FREE SPACE AND ON BODY

A. FREE SPACE

The presented antenna was placed over a 3 × 3 array of HIS structures. The configuration of integration is revealed in Fig.8. To avoid short circuits, a foam with a thickness of 1 mm is inserted between them. It is worth mentioning that the addition of an antenna to HIS caused mutual impedance coupling between them [7] which can cause resonant frequency detuning. Therefore, to obtain the desired band of 2.45 GHz, the antenna ground was modified when incorporated with the HIS structures. The length of the ground plane (Lg) was modified from 2.7 mm to 15 mm. The prototypes are shown in Fig.9.

Fig.10 discloses the simulated and measured results of the combining presented antenna with HIS. The results show that both of them maintained reflection coefficient below −10 dB in the broad agreement. There is a slight shift in the measured result, which could result from manufacturing errors. The results also show that the integrated design reveals a better reflective coefficient than the antenna alone in Fig.4.

The radiation patterns of antenna alone and antenna with HIS is shown in Fig.11. It shows that the HIS-free antenna has the maximum back radiation that could be considered a health
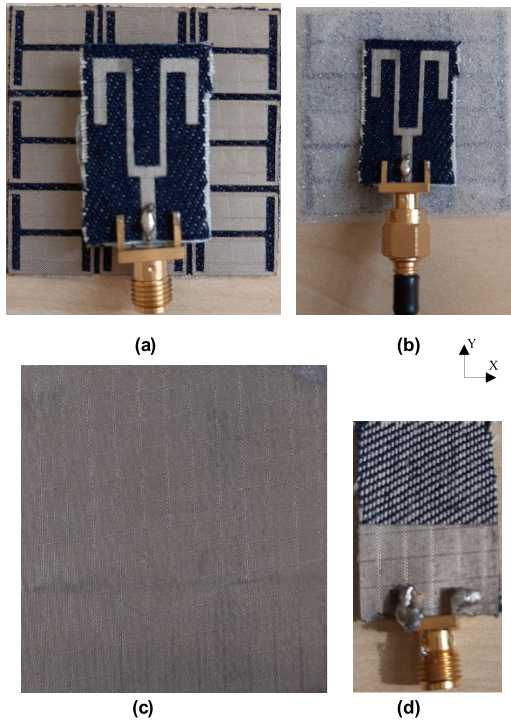
FIGURE 9. Prototype of the integrated antenna with HIS (a) with foam, (b) without foam, (c) back view HIS, and (d) back view antenna.
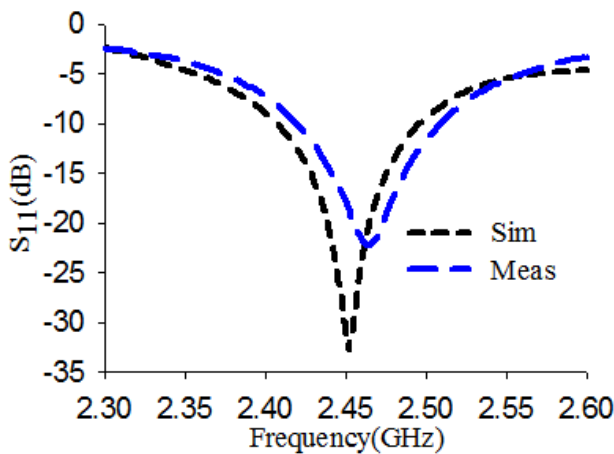

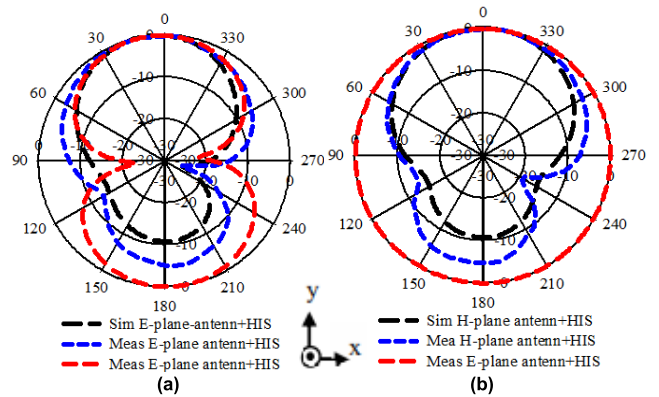**FIGURE 10.** S_{11} of the antenna with HIS.

FIGURE 11. Comparison normalized radiation pattern between the antenna alone and with HIS (a) E-plane, and (b) H-plane.
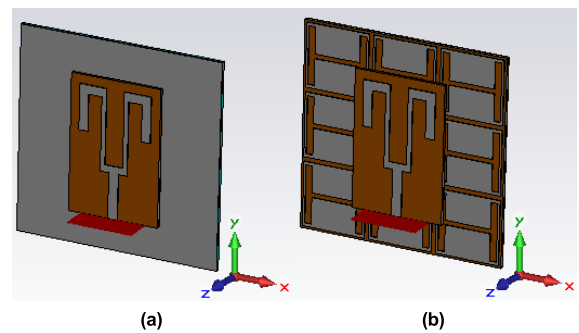

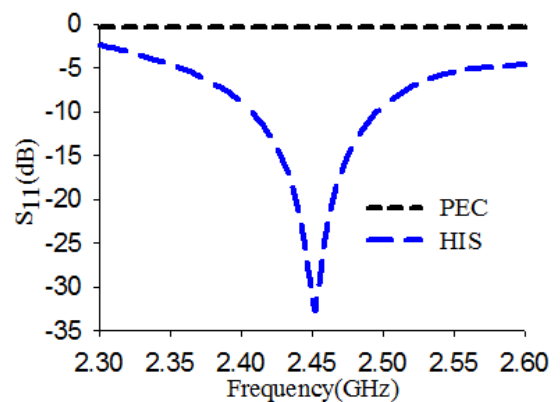**FIGURE 12.** Presented antenna over (a) PEC, and (a) HIS.

FIGURE 13. S_{11} of antenna over PEC and HIS.

risk [7, 36]. However, the addition of HIS to the antenna reduced the back radiation by 10.8 dB. It also improved the antenna gain from 1.96 dBi to 7.47 dBi and maintained efficiency of 71.8%.

B. COMPARISON BETWEEN HIS AND PERFECT ELECTRIC CONDUCTOR (PEC)

We perform a comparison between the use of HIS and PEC as ground planes. In theoretical terms, the PEC has an infinite conductivity, σ (S / m). However, there are products such as copper with a finite conductivity that can be approximated as PEC. Copper conductivity is 5.8×10^7 S / m. For a fair

comparison, the antenna was mounted above the PEC and HIS with the same height and dimensions as shown in Fig.12.

Fig.13 presents the performance in both cases as a ground plane below the antenna. The result shows that the coefficient of reflection for the PEC case is detuned; in other words, the frequency of resonance is not shown. According to image theory [37], when an antenna is very close to the PEC, the reverse image current is produced. The current picture in the PEC cancels the current in the antenna, so the output of the antenna drops and becomes very low. This process is called destructive. In order to solve this problem,
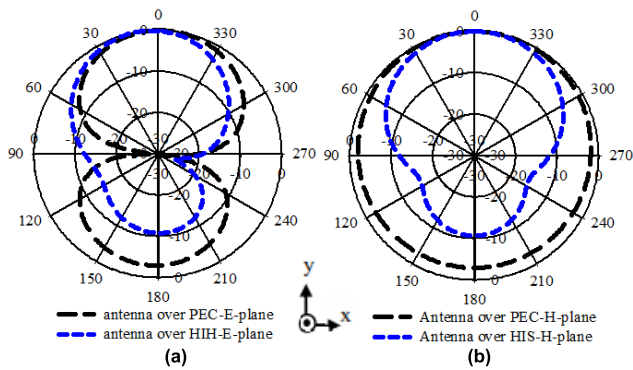
FIGURE 14. Normalized radiation pattern of presented antenna over PEC and HIS (a) E-plane, and (b) H-plane.

it is necessary to detach the antenna from the PEC at least λ/4 of the operating wavelength. However, the overall size includes a minimum thickness of λ/4, limiting its applications in low-profile antenna designs. A strong reflecting coefficient is realized on the desired band when the antenna is positioned over HIS. This is due to HIS's capability to cause the image current to be in the same direction as the antenna current [38].

The normalized pattern of radiation in both cases was also compared, as shown in Fig.14. It can be shown that the HIS antenna decreases the back radiation compared to the PEC antenna. As a result, the harmful impacts due to the backward radiation of the antenna would be very minimal in the case of the integration of the antenna with HIS.

It should be noted that by integrating the HIS with the wearable antenna, not only the physical properties of the antenna can be enhanced in such a way that the geometry of the antenna is smaller and low-profile, but the radiation properties of the antenna can also be significantly improved in terms of front to back ratio, gain, directivity and pattern of radiation. The HIS will also minimize the back radiation to the body, minimizing lossy's body degradation on the wearable antenna's output. The wearable antenna can therefore work equally well, whether it is positioned off/on the body. We also compared the efficiency of the antenna over PEC, HIS in terms of gain and FBR. Fig.15 displays the findings. It can be shown that the PEC antenna has low FBR suggesting high back radiation to the body that can cause health problems. Whereas, the antenna above HIS displays strong FBR, suggesting low back radiation to the body. Besides, the antenna HIS shows a much better gain of 7.48 dBi than the antenna over PEC, which shows a gain of 3.48 dBi, as shown in Fig.15.

C. BENDING

To evaluate the robustness of the integrated HIS with antenna, bending sensitivity studies have been conducted to evaluate the design performance. The investigation is conducted numerically and experimentally along the y-axis and x-axis, as shown in Fig.16 and Fig.17. Several diameters, including 60 mm, 80 mm, 100 mm and 140 mm, are selected for the
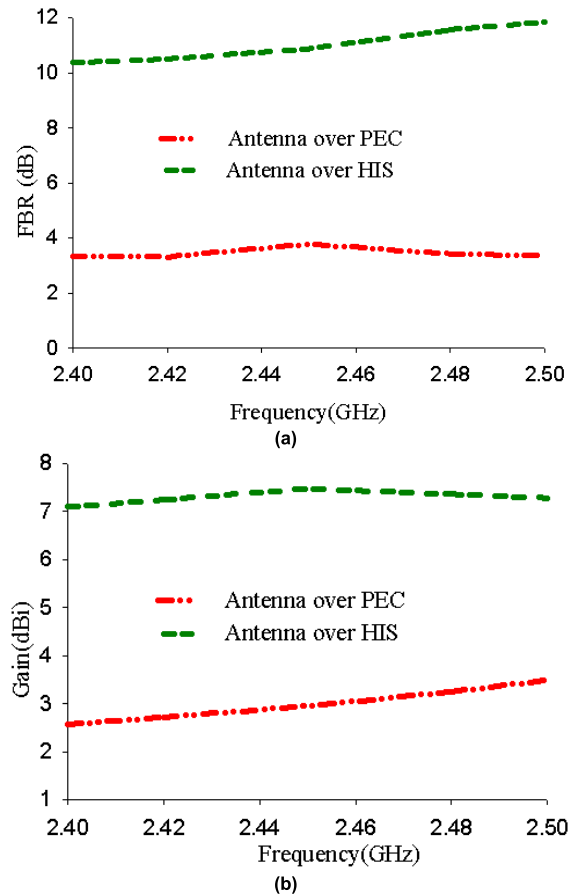

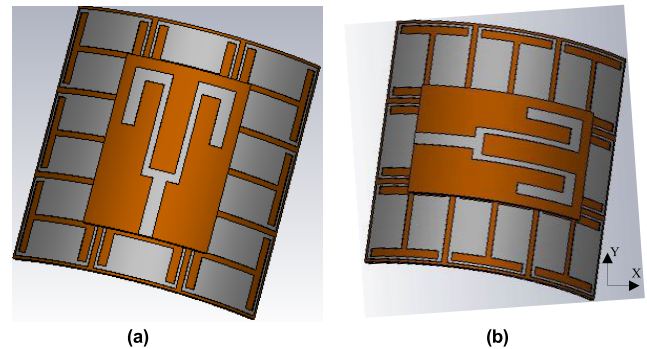**FIGURE 15.** Performance of the antenna over PEC and HIS (a) FBR, and (b) Gain.

FIGURE 16. Bending of the antenna with HIS (simulation) (a) y-axis, and (b) x-axis.

design assessment. The selected diameters are based on the typical size of human arms and legs.

Fig.18 and 19 illustrate the simulated and measured bending results along both the y-axis and the x-axis, respectively. Generally, the desired resonant frequency of 2.45 GHz is achieved in all variable diameters below – 10 dB, even at extreme bending levels.

It can be seen that, in the two cases of y-axis and x-axis, the effect of bending is that the resonance frequency is shifted upwards by about 15 dB compared to the flat case. Also, in the case of the y-axis, it can be seen that the resonance
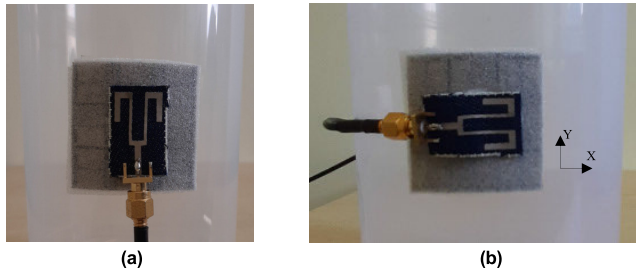
FIGURE 17. Bending of the antenna with HIS (measurement) (a) y-axis, and (b) x-axis.
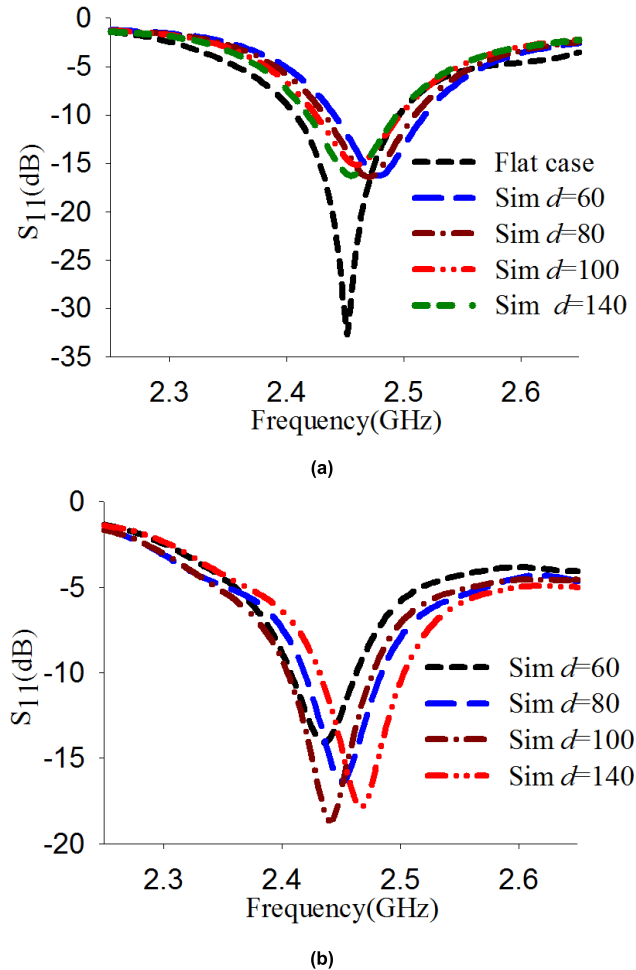

FIGURE 18. Evaluation of the design performance under bending along y-axis (a) Simulation, and (b) measurement.

FIGURE 19. Evaluation of the design performance under bending along x-axis (a) Simulation, and (b) measurement.

Furthermore, the radiation patterns along the four diameters also studied during the simulation from 60 mm to 140 mm, while measured along 140 mm as presented in Fig.20. It is seen that the normalized radiation pattern in free space and along the four diameters are comparable. There are slight increments in the back radiation compared to the flat case. This could occur due to minor effects of bending on conduction materials. The gain of the presented antenna with the HIS in both cases is within the range of 4.67 dBi and 7 dBi. Furthermore, the radiated efficiency at an extreme degree of bending is maintained above 65.3 %. Hence, the presented design is robust and suitable for wearable applications.

D. ON BODY
Since the presented integrated HIS with antenna is used for worn purposes, the effect of the body on the integrated design performance was investigated. Two types of numerical phantoms models are developed. They are chest and arm, as depicted in Fig.21. Each model consists of four layers they are bone, muscle, fat, and skin. Their data and thickness have been taken from [7], [20], [39], [40]. The design was investigated by placing it directly on the skin and assuming that the worn clothes have a thickness of 1 mm, 2 mm and

frequency has shifted slightly to higher frequencies as the diameter drops to 60 mm. In the case of the x-axis, it can be seen that the resonance frequency is slightly shifted to lower frequencies as the diameter is reduced to 60 mm. The effect is considered to be negligible, however, as the −10 dB bandwidth still covers the required 2.45 GHz, frequency band. The simulated result is seen to be more stable compared to the measured results; this could be due to the use of plastic cylinders as well as manufacturing errors, cables and connectors.
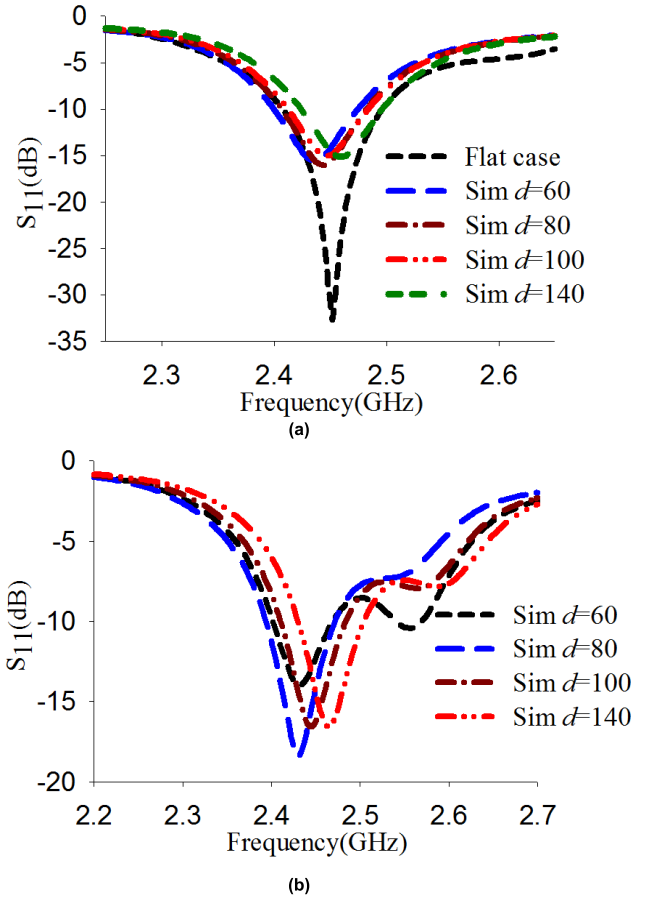
FIGURE 20. Bending evolution (a) y-axis (b) x-axis.

FIGURE 21. (a) Chest mode, and (b) Arm model.

FIGURE 22. Performance of the antenna with HIS loading on (a) Chest and (b) Arm.
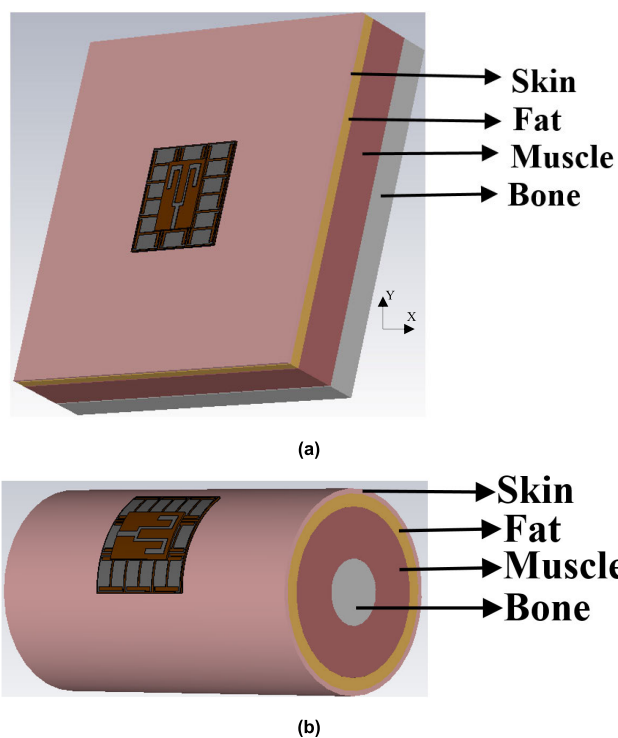
3 mm. To show the HIS's usefulness to the antenna design, the antenna also investigated with the same positions.

Fig.22 depicts the results of the antenna with HIS loaded on chest and arm. It is observed that when the antenna with HIS, the desired band is achieved even when the integrated design placed directly on the skin. The slight shift for the case directly on the skin is negligible since the 2.45 GHz is still within the −10 dB.

On the other hand, placing the antenna alone (without HIS) on the body with the same positions as in Fig.22 is affected, as shown in Fig.23. The S_{11} shifted to the lower band, especially for the case when directly loaded on the skin. This is due to the high conductivity of the model, which acts as an additional ground for the antenna. Based on this result, it can be concluded that with the introduction of HIS,
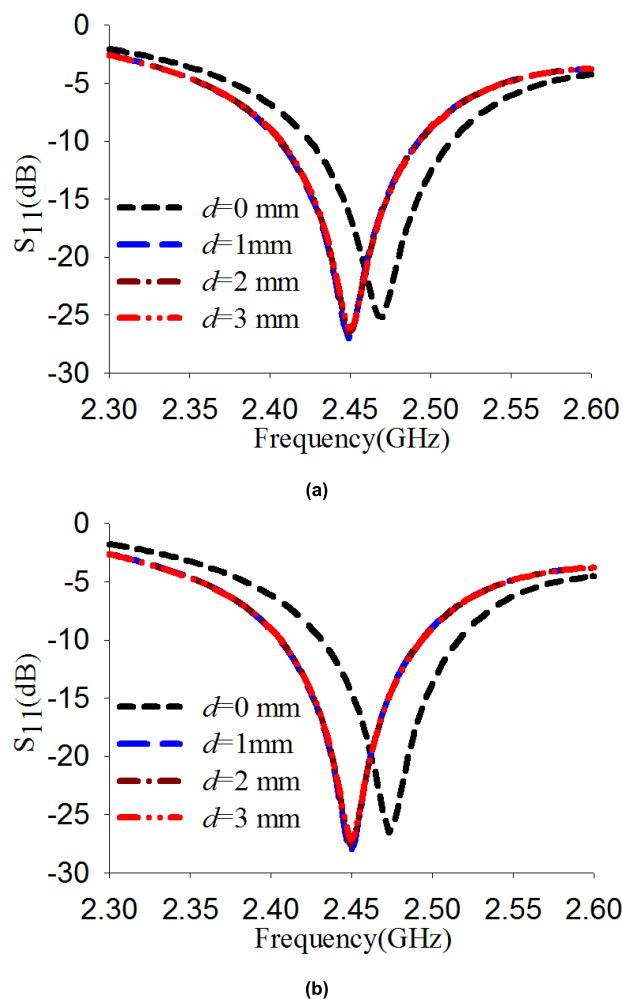
the performance of the antenna is maintained as the case of free space.

Fig.24and 25 show the radiation patterns of the antenna alone and with HIS when loaded onto the body. It is seen that when the antenna is alone and compared to free space, the back radiation is reduced by 10 dB, indicating the amount of energy absorbed by the body, which may pose a health risk [7], [36]. However, adding HIS reveals comparable results with the case without the loading body, indicating the benefits of HIS acting as an insulation between the antenna and the body. As a result, it will protect the body from the harmful radiation that may pose a health risk.

The proposed integrated antenna with HIS has also been experimentally studied. The experiment was performed on a male volunteer with a weight and height of 76 kg and 160 cm, respectively, as shown in Fig.26. The design was loaded into four parts: the chest, the back, the thigh, and the arm. The S_{11} is shown in Fig.27. Overall, the bandwidth of −10 dB applies to the desired resonant frequency of 2.45 GHz in all cases. There is a slight shift on the S_{11} in the case of the arm.
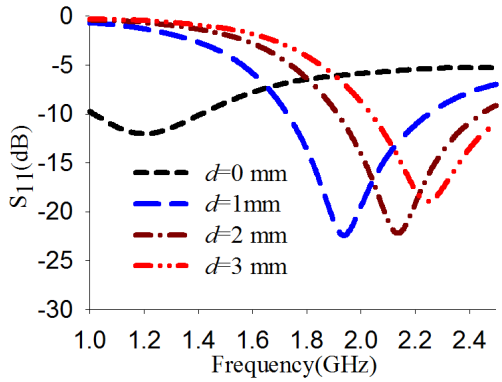
(a)
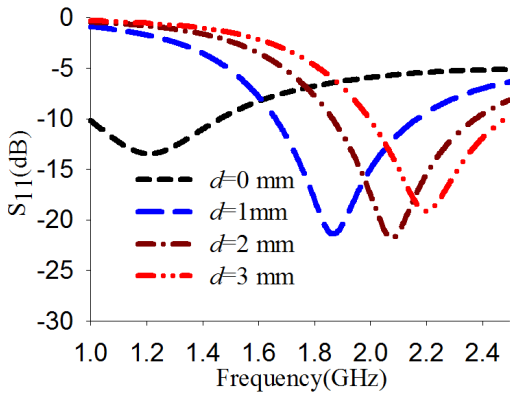
(b)

FIGURE 23. Performance of the antenna without HIS loading on (a) Chest and (b) Arm.

(a)   **(b)**
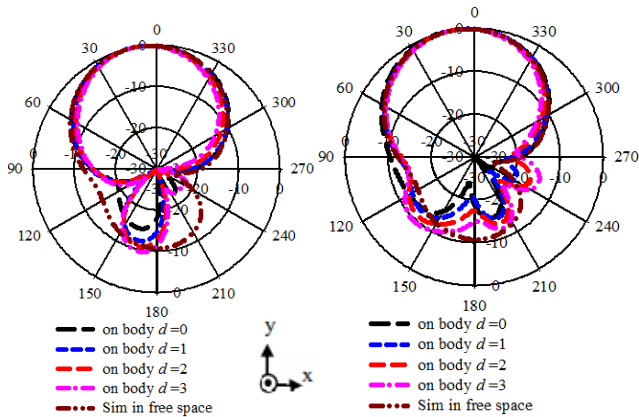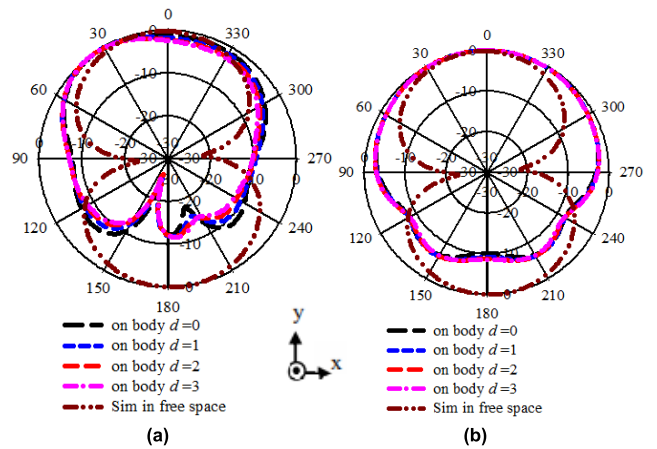
FIGURE 24. Normalized radiation pattern of the antenna with HIS loading on (a) Chest and (b) Arm.

It could be due to a bend along the arm, but it is negligible as the bandwidth is still within −10 dB of 2.45 GHz.

E. SAR

Since the proposed antenna (with and without HIS) operates close to the human body, SAR is an important parameter for evaluation. Generally, the mass average SAR is calculated and compared to exposure limits established by regulatory standards to prevent human tissues from being at

(a)   **(b)**

FIGURE 25. Normalized radiation pattern of the antenna without HIS loading on (a) Chest and (b) Arm.

(a)   **(b)**

(c)   **(d)**

FIGURE 26. Proposed integrated antenna with HIS on several parts of the body (a) Chest, (b) Back, (c) Thigh, and (d) Arm.

TABLE 3. SAR values of the antenna alone and with HIS.

Distance from the tissue models	Antenna (SAR level W/kg)		Antenna+HIS (SAR level W/kg)	
	chest	arm	chest	arm
0	7.8	10.3	0.133	0.069
1	7.51	8.64	0.0257	0.036
2	6.18	7.13	0.0209	0.293
3	5.77	6.7	0.018	0.223

risk [7], [36]. Therefore, simulations have been conducted for both cases with and without HIS to ensure the safety level of SAR that meets the limit set by FCC, which should be less than 1.6 W/ kg above 1 g on average [7], [19], [20], [21].

The SAR simulation performed based on IEEE C95.1 available in CST. The input power is set at 100 mW as a benchmark. The same phantom models developed in Section 4C are used for the SAR study. The SAR levels were investigated when the design was placed directly on the model
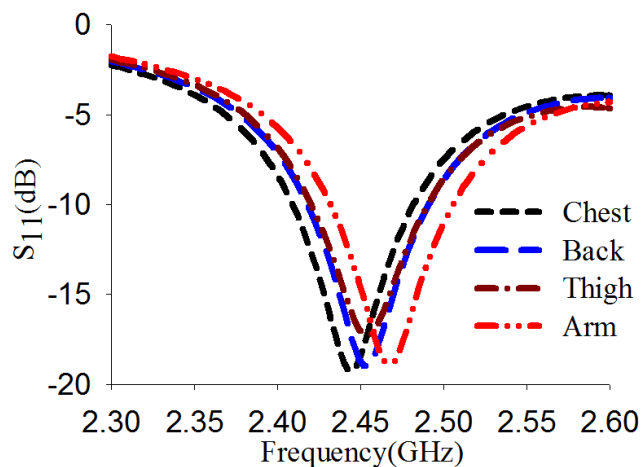
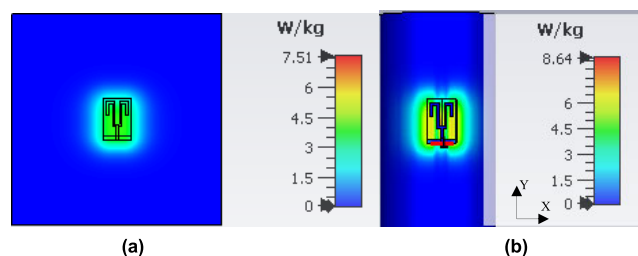**FIGURE 27.** Performance of the antenna with HIS loading on human body.

FIGURE 28. SAR level of the antenna without HIS at 1 mm far from the phantoms (a) Chest, and (b) Arm.
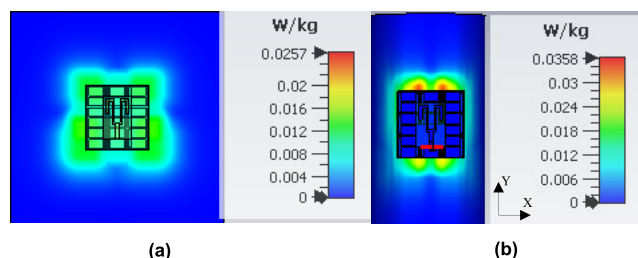

FIGURE 29. SAR level of the antenna with HIS at 1 mm far from the phantoms (a) Chest, and (b) Arm.

and at varying distances between the model and the body. The results are summarized in Table 3. It is seen that when the antenna is alone, the level of SAR exceeds the safety level event when the antenna is placed 3 mm away from the models. However, the addition of HIS to the antenna shows that the SAR level complies with the safety level. The level is much lower than the safety level, even when the integrated design is placed directly on the body. It proves the usefulness of introducing HIS in the design of the wearable antenna. Fig. 28 and Fig.29 present the 3D results at 1 mm away from the phantom models.

F. WORST CASE STUDY
We have also carried out a study on the impact of varying the body phantom's permittivity to examine the performance, functionality, and robustness of the presented antenna on its own and add HIS in terms of reflective coefficient stability
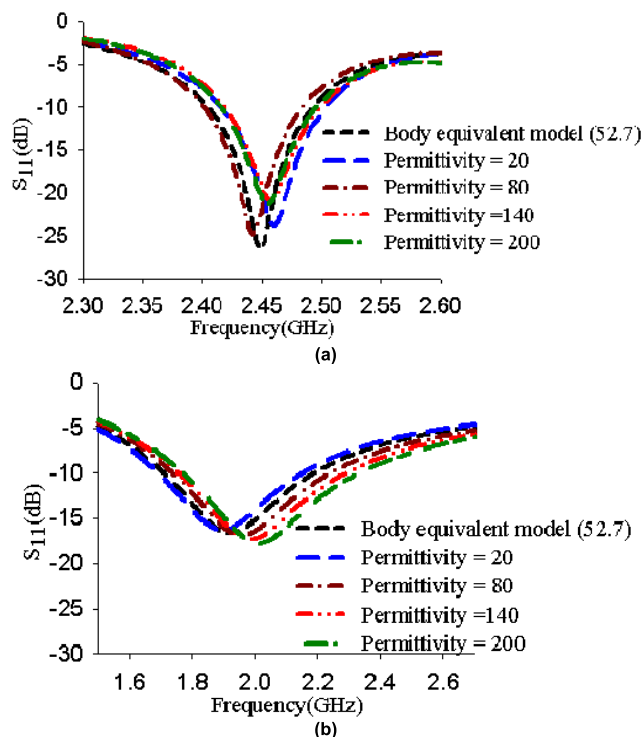
FIGURE 30. SAR level of the antenna without HIS at 1 mm far from the phantoms (a) Chest, and (b) Arm.

TABLE 4. SAR values with varying the permittivity values.

Permittivity	20	52.7	80	140	200
Antenna with HIS	0.0445	0.0569	0.0659	0.084	0.0794
Antenna alone	17.9	16.7	17.2	16.1	15

TABLE 5. Performance summary of the antennas with and without HIS.

Designs	Profile (mm)	Area (mm^2)	SAR w/kg	Gain (dBi)	FBR (dB)	Stability of S$_{11}$ on body
Antenna alone	0.7	30×20	7.51	1.96	0	Shifted to lower band
Antenna with HIS	2.4	45×45	0.0257	7.47	10.8	Stable at 2.45 GHz

and SAR levels. An equivalent body model with a scale of $150 \times 150 \times 40$ mm^3, an output of 52.7, and a conductivity of 1.95 Δ (S / m) at 2.45 GHz [41] are used. The permittivity values selected were 20, 52.7, and 80,140,200. The antenna with and without HIS was mounted at a distance of 1 mm from the phantom model. Fig.30 displays the effects of the coefficient of reflection. Variation of the permittivity values has been found to have affected the reflection coefficient of the antenna alone. This is because the model would serve as an additional substrate to the antenna, allowing the reflection coefficient to transfer to lower bands even at 20. In contrast, HIS's addition demonstrates an excellent stable reflection coefficient even at a high permittivity of 200. It shows that the HIS serves as isolation between the body and the antenna.

TABLE 6. Comparison of the proposed antenna with the recent wearable antennas design in WBAN.

Ref	Year	No. of unit cell	Profile (mm)	Area(mm^2)	SAR(W/KG)	Gain (dBi)	Efficiency (%)	Substrate type
[15]	2018	3×3	4	81×81	0.230	7.3	71	Fabric
[27]	2019	-	6	70×85	-	8.3	49	Felt
[20]	2020	2×2	2.4	60×60	0.983	6.45	72.3	Jeans
[28]	2020	1×2	5	50×25.7	0.521	4.06	44.39	Felt
[29]	2020	3×3	5.28	85.5×85.5	0.111	1.94	-	Felt
[30]	2020	4×3	3.424	145×112	-	6.19	61	Jeans
[31]	2020	2×2	6	56×56	0.22	6.51	74.8	Ultralam850,Felt
[32]	2020	3×3	8.5	60×60	0.612	6.56	70.7	PDMS
This design	2021	3×3	2.4	45×45	0.0257	7.47	71.8	Jeans

The SAR level was investigated with varying the permittivity Body equivalent model. The results are tabulated in Table 4 for both cases; it is realized that when the antenna alone the SAR level does not comply with standard set by FCC even at low permittivity of 20, while integrating antenna with HIS, the SAR level comply with standards even at high permittivity of 200. Hence, the integrated antenna with HIS is mechanically robust to human body tissue loading, and it is highly appropriate for body-worn applications.

V. CONCLUSION

The antenna for wearable medical applications is successfully presented with a full fabric high impedance surface. The overall size of the HIS antenna is 45× 45 × 2.4 mm^3 (0.37λo×0.37λo×0.02 mm^3). The antenna alone was studied in free space and on the body and showed that the S$_{11}$ was detuned when placed on the body due to the high conductivity of the body. HIS was therefore introduced because it could isolate the antenna from the body and maintain its performance compared to free space. Besides, the HIS antenna showed a robust result when it was mounted on the body and flexed. It has achieved a gain of 7.47, FBR of 10.8, an efficiency of 71.8% per cent and reduces the SAR below the safety limits. The reduction is more than 95%. Therefore, the design presented considers that it is suitable for wearable applications. Finally, the performance of the integrated design with the antenna alone and with some other WBAN wearable antennas is compared, as shown in Tables V and VI, respectively. Further study was also performed to show the useful of placing antenna over HIS compared to the use of perfect electric conductor (PEC). The integrated design was also investigated with the worst case of varying the permittivity of body equivalent model which shows excellent performance in term of reflection coefficient and SAR levels. Hence, the integrated antenna with HIS is mechanically robust to human body tissue loading, and it is highly appropriate for body-worn applications. Generally, the proposed design shows better performance and can be considered a promising candidate for human wearable devices.

REFERENCES

[1] A. Kamalaveni and M. Ganesh Madhan, "A compact TRM antenna with high impedance surface for SAR reduction at 1800 MHz," *AEU-Int. J. Electron. Commun.*, vol. 70, no. 9, pp. 1192–1198, Sep. 2016.

[2] A. Y. I. Ashyap, W. N. N. W. Marzudi, Z. Z. Abidin, S. H. Dahlan, H. A. Majid, and M. R. Kamaruddin, "Antenna incorporated with electromagnetic bandgap (EBG) for wearable application at 2.4 GHz wireless bands," in *Proc. IEEE Asia–Pacific Conf. Appl. Electromagn. (APACE)*, 2016, pp. 217–221.

[3] A. A. Abdel Aziz, A. T. Abdel-Motagaly, A. A. Ibrahim, W. M. A. El Rouby, and M. A. Abdalla, "A printed expanded graphite paper based dual band antenna for conformal wireless applications," *AEU-Int. J. Electron. Commun.*, vol. 110, Oct. 2019, Art. no. 152869.

[4] A. Y. I. Ashap, Z. Z. Abidin, S. H. Dahlan, H. A. Majid, S. K. Yee, G. Saleh, and N. Abdul Malek, "Flexible wearable antenna on electromagnetic band gap using PDMS substrate," *Telkomnika (Telecommun. Comput. Electron. Control)*, vol. 15, no. 3, p. 1454, Sep. 2017.

[5] S. A. Kumar and T. Shanmuganantham, "Design and analysis of implantable CPW fed bowtie antenna for ISM band applications," *AEU-Int. J. Electron. Commun.*, vol. 68, no. 2, pp. 158–165, Feb. 2014.

[6] S. Ashok Kumar and T. Shanmuganantham, "Design of implantable CPW fed monopole H-slot antenna for 2.45GHz ISM band applications," *AEU-Int. J. Electron. Commun.*, vol. 68, no. 7, pp. 661–666, Jul. 2014.

[7] A. Y. I. Ashyap, Z. Zainal Abidin, S. H. Dahlan, H. A. Majid, M. R. Kamarudin, A. Alomainy, R. A. Abd-Alhameed, J. S. Kosha, and J. M. Noras, "Highly efficient wearable CPW antenna enabled by EBG-FSS structure for medical body area network applications," *IEEE Access*, vol. 6, pp. 77529–77541, 2018.

[8] M. Karimyian-Mohammadabadi, M. A. Dorostkar, F. Shokuohi, M. Shanbeh, and A. Torkan, "Super-wideband textile fractal antenna for wireless body area networks," *J. Electromagn. Waves Appl.*, vol. 29, no. 13, pp. 1728–1740, Sep. 2015.

[9] P. M. Potey and K. Tuckley, "Design of wearable textile antenna for low back radiation," *J. Electromagn. Waves Appl.*, vol. 34, no. 2, pp. 235–245, Jan. 2020.

[10] W. El Hajj, C. Person, and J. Wiart, "A novel investigation of a broadband integrated Inverted-F antenna design; application for wearable antenna," *IEEE Trans. Antennas Propag.*, vol. 62, no. 7, pp. 3843–3846, Jul. 2014.

[11] I. Gil and R. Fernández-García, "Wearable PIFA antenna implemented on jean substrate for wireless body area network," *J. Electromagn. Waves Appl.*, vol. 31, nos. 11–12, pp. 1194–1204, Aug. 2017.

[12] M. N. Suma, P. C. Bybi, and P. Mohanan, "A wideband printed monopole antenna for 2.4-GHz WLAN applications," *Microw. Opt. Technol. Lett.*, vol. 48, no. 5, pp. 871–873, May 2006.

[13] H. Memarzadeh-Tehran, R. Abhari, and M. Niayesh, "A cavity-backed antenna loaded with complimentary split ring resonators," *AEU-Int. J. Electron. Commun.*, vol. 70, no. 7, pp. 928–935, Jul. 2016.

[14] H. R. Raad, A. I. Abbosh, H. M. Al-Rizzo, and D. G. Rucker, "Flexible and compact AMC based antenna for telemedicine applications," *IEEE Trans. Antennas Propag.*, vol. 61, no. 2, pp. 524–531, Feb. 2013.

[15] G.-P. Gao, B. Hu, S.-F. Wang, and C. Yang, "Wearable circular ring slot antenna with EBG structure for wireless body area network," *IEEE Antennas Wireless Propag. Lett.*, vol. 17, no. 3, pp. 434–437, Mar. 2018.

[16] T. A. Elwi, H. M. Al-Rizzo, D. G. Rucker, and H. R. Khaleel, "Effects of twisting and bending on the performance of a miniaturized truncated sinusoidal printed circuit antenna for wearable biomedical telemetry devices," *AEU-Int. J. Electron. Commun.*, vol. 65, no. 3, pp. 217–225, Mar. 2011.

[17] W. A. Awan, N. Hussain, and T. T. Le, "Ultra-thin flexible fractal antenna for 2.45 GHz application with wideband harmonic rejection," *AEU-Int. J. Electron. Commun.*, vol. 110, Oct. 2019, Art. no. 152851.

[18] M. A. B. Abbasi, S. S. Nikolaou, M. A. Antoniades, M. Nikolic Stevanovic, and P. Vryonides, "Compact EBG-backed planar monopole for BAN wearable applications," *IEEE Trans. Antennas Propag.*, vol. 65, no. 2, pp. 453–463, Feb. 2017.

[19] Z. H. Jiang, D. E. Brocker, P. E. Sieber, and D. H. Werner, "A compact, low-profile metasurface-enabled antenna for wearable medical body-area network devices," *IEEE Trans. Antennas Propag.*, vol. 62, no. 8, pp. 4021–4030, Aug. 2014.

[20] A. Y. I. Ashyap, S. H. B. Dahlan, Z. Z. Abidin, M. H. Dahri, H. A. Majid, M. R. Kamarudin, S. K. Yee, M. H. Jamaluddin, A. Alomainy, and Q. H. Abbasi, "Robust and efficient integrated antenna with EBG-DGS enabled wide bandwidth for wearable medical device applications," *IEEE Access*, vol. 8, pp. 56346–56358, 2020.

[21] Z. H. Jiang, Z. Cui, T. Yue, Y. Zhu, and D. H. Werner, "Compact, highly efficient, and fully flexible circularly polarized antenna enabled by silver nanowires for wireless body-area networks," *IEEE Trans. Biomed. Circuits Syst.*, vol. 11, no. 4, pp. 920–932, Aug. 2017.

[22] K. Kamardin, M. K. A. Rahim, P. S. Hall, N. A. Samsuri, T. A. Latef, and M. H. Ullah, "Planar textile antennas with artificial magnetic conductor for body-centric communications," *Appl. Phys. A, Solids Surf.*, vol. 122, no. 4, p. 363, Apr. 2016.

[23] A. Y. I. Ashyap, Z. Zainal Abidin, S. H. Dahlan, H. A. Majid, and G. Saleh, "Metamaterial inspired fabric antenna for wearable applications," *Int. J. RF Microw. Comput.-Aided Eng.*, vol. 29, no. 3, Mar. 2019, Art. no. e21640.

[24] S. Velan, E. F. Sundarsingh, M. Kanagasabai, A. K. Sarma, C. Raviteja, R. Sivasamy, and J. K. Pakkathillam, "Dual-band EBG integrated monopole antenna deploying fractal geometry for wearable applications," *IEEE Antennas Wireless Propag. Lett.*, vol. 14, pp. 249–252, 2015.

[25] B. Hazarika, B. Basu, and J. Kumar, "A multi-layered dual-band on-body conformal integrated antenna for WBAN communication," *AEU-Int. J. Electron. Commun.*, vol. 95, pp. 226–235, Oct. 2018.

[26] A. Al-Sehemi, A. Al-Ghamdi, N. Dishovsky, N. Atanasov, and G. Atanasova, "On-body investigation of a compact planar antenna on multilayer polymer composite for body-centric wireless communications," *AEU-Int. J. Electron. Commun.*, vol. 82, pp. 20–29, Dec. 2017.

[27] Sanchez-Montero, Lopez-Espi, Alen-Cordero, and Martinez-Rojas, "Bend and moisture effects on the performance of a U-Shaped slotted wearable antenna for off-body communications in an industrial scientific medical (ISM) 2.4 GHz band," *Sensors*, vol. 19, no. 8, p. 1804, Apr. 2019.

[28] M. El Atrash, M. A. Abdalla, and H. M. Elhennawy, "A compact flexible textile artificial magnetic conductor-based wearable monopole antenna for low specific absorption rate wrist applications," *Int. J. Microw. Wireless Technol.*, pp. 1–7, Jun. 2020.

[29] R. Joshi, E. F. N. M. Hussin, P. J. Soh, M. F. Jamlos, H. Lago, A. A. Al-Hadi, and S. K. Podilchak, "Dual-band, dual-sense textile antenna with AMC backing for localization using GPS and WBAN/WLAN," *IEEE Access*, vol. 8, pp. 89468–89478, 2020.

[30] M. M. Bait-Suwailam, I. I. Labiano, and A. Alomainy, "Impedance enhancement of textile grounded loop antenna using high-impedance surface (HIS) for healthcare applications," *Sensors*, vol. 20, no. 14, p. 3809, Jul. 2020.

[31] M. El Atrash, M. A. Abdalla, and H. M. Elhennawy, "A compact highly efficient ∏-section CRLH antenna loaded with textile AMC for wireless body area network applications," *IEEE Trans. Antennas Propag.*, early access, Jul. 27, 2020, doi: 10.1109/TAP.2020.3010622.

[32] G. Gao, S. Wang, R. Zhang, C. Yang, and B. Hu, "Flexible EBG-backed PIFA based on conductive textile and PDMS for wearable applications," *Microw. Opt. Technol. Lett.*, vol. 62, no. 4, pp. 1733–1741, Apr. 2020.

[33] P. K. Panda and D. Ghosh, "Wideband and high gain tuning fork shaped monopole antenna using high impedance surface," *AEU-Int. J. Electron. Commun.*, vol. 111, Nov. 2019, Art. no. 152920.

[34] A. Y. I. Ashyap, S. H. B. Dahlan, Z. Zainal Abidin, M. I. Abbasi, M. R. Kamarudin, H. A. Majid, M. H. Dahri, M. H. Jamaluddin, and A. Alomainy, "An overview of electromagnetic band-gap integrated wearable antennas," *IEEE Access*, vol. 8, pp. 7641–7658, 2020.

[35] Shivnarayan, S. Sharma, and B. R. Vishvakarma, "Analysis of slot-loaded rectangular microstrip patch antenna," *Ind. J. Radio Space Phys.*, vol. 34, pp. 424–430, Dec. 2005.

[36] S. Yan, P. J. Soh, and G. A. E. Vandenbosch, "Low-profile dual-band textile antenna with artificial magnetic conductor plane," *IEEE Trans. Antennas Propag.*, vol. 62, no. 12, pp. 6487–6490, Dec. 2014.

[37] C. A. Balanis, *Antenna Theory: Analysis and Design*, 3rd ed. Hoboken, NJ, USA: Wiley, 2005, p. 1117.

[38] D. Sievenpiper, L. Zhang, R. F. J. Broas, N. G. Alexopolous, and E. Yablonovitch, "High-impedance electromagnetic surfaces with a forbidden frequency band," *IEEE Trans. Microw. Theory Techn.*, vol. 47, no. 11, pp. 2059–2074, 1999.

[39] A. Y. I. Ashyap, Z. Zainal Abidin, S. H. Dahlan, H. A. Majid, S. M. Shah, M. R. Kamarudin, and A. Alomainy, "Compact and low-profile textile EBG-based antenna for wearable medical applications," *IEEE Antennas Wireless Propag. Lett.*, vol. 16, pp. 2550–2553, 2017.

[40] *Body Tissue Dielectric Parameters Tool*. Accessed: Dec. 10, 2019. [Online]. Available: http://www.fcc.gov/encyclopedia/bodytissue-dielectric-parameters

[41] J. Gemio, J. Parron, and J. Soler, "Human body effects on implantable antennas for ism bands applications: Models comparison and propagation losses study," *Prog. Electromagn. Res.*, vol. 110, pp. 437–452, Nov. 2010.

ADEL Y. I. ASHYAP received the B.Eng., M.Eng. and Ph.D. degrees in electrical engineering from Universiti Tun Hussein Onn Malaysia (UTHM), Malaysia, in 2012, 2014, and 2019, respectively. He is currently a Postdoctoral Fellow with the Research Center of Applied Electromagnetics, Faculty of Electrical and Electronic Engineering, UTHM. He has authored and coauthored numbers of journals and proceedings. His research interests include electromagnetic bandgap (EBG), artificial magnetic conductor (AMC) for wireless body area networks (WBAN), microstrip antennas, and small antennas for biomedical devices. He was received the Chancellor Award for his final year project and a number of Gold, Silver, and Bronze medals in international and local competitions.

SAMSUL HAIMI BIN DAHLAN received the Ph.D. degree in signal processing and telecommunications from the Universite de Rennes 1, France, in 2012. He has been a Senior Lecturer with the Faculty of Electrical and Electronic Engineering, Universiti Tun Hussein Onn Malaysia (UTHM), since March 2012. He is currently a Principal Researcher with the Research Center for Applied Electromagnetics (EMCenter, UTHM) and appointed as the Head of the Center, since April 2015. He has authored and coauthored numbers of journals, including the IEEE Transaction on Electromagnetic Compatibility and IEEE Antennas and Wireless Propagation Letters (AWPL). He is supervising a numbers of Ph.D., master's, and bachelor's students and involved in several research projects sponsored by the industry and government agencies. His research interests include optical-microwave generator, focusing systems (dielectric lens and transmitarray's synthesis), and computational electromagnetic technique namely the BOR-FDTD and material characterizations.

ZUHAIRIAH ZAINAL ABIDIN (Member, IEEE) received the Ph.D. degree from Bradford University, U.K., in 2011. She is currently the Head of the Research Center of Wireless and Radio Science (WARAS), Faculty of Electrical and Electronic Engineering, Universiti Tun Hussein Onn Malaysia. She has authored and coauthored numbers of journals and proceedings. Her research interests include MIMO antenna, printed microstrip antenna, wearable antennas, meta-material resonator, electromagnetic bandgap (EBG) for wireless and mobile, and high-speed digital circuit's applications.

SHARUL KAMAL ABDUL RAHIM (Senior Member, IEEE) received the bachelor's degree in electrical engineering from The University of Tennessee, Knoxville, TN, USA, in 1996, the M.Sc. degree in engineering (communication engineering) from Universiti Teknologi Malaysia (UTM), in 2001, and Ph.D. degree in wireless communication system from the University of Birmingham, U.K., in 2007. He is currently a Professor with the Wireless Communication Centre, Faculty of Electrical Engineering, UTM Skudai. He is also a member of the IEEE Malaysia Section, a Member Board of Engineer Malaysia (MBEM), a member of the Institute of Engineer Malaysia (MIEM), and an Eta Kappa Nu Chapter (International Electrical Engineering Honor Society, University of Tennessee). He has published more than 50 journal articles and technical proceedings on rain attenuations, smart antenna systems, microwave design, and reconfigurable antenna in national and international journals and conferences. His research interest includes smart antenna on communication systems.

HUDA A. MAJID (Member, IEEE) received the B.Eng. degree in electrical engineering (telecommunication), and the M.Eng. and Ph.D. degrees in electrical engineering from Universiti Teknologi Malaysia, in 2007, 2010, and 2013, respectively. He is currently a Lecturer with the Department of Electrical Engineering Technology, Faculty of Engineering Technology, Universiti Tun Hussein Onn Malaysia. He has published over 50 articles in journal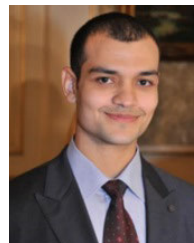s and conference papers. His research interests include design of microstrip antennas, small antennas, reconfigurable antennas, metamaterials structure, metamaterial antennas, and millimeter wave antennas.

ABDULRAHMAN S. M. ALQADAMI (Graduate Student Member, IEEE) received the B.Eng. (Hons.) and M.Sc.Eng. degrees in communication engineering from University Malaysia Perlis (UniMAP), Malaysia, in 2013 and 2016, respectively. He is currently pursuing the Ph.D. degree with the Electromagnetic Innovations (εMAGin) Group, School of Information Technology and Electrical Engineering, The University of Queensland, Australia. His current research interests include flexible antennas for electromagnetic imaging applications, meta-material antennas, development and characterization of composite dielectric substrate materials, and wearable sensors for different biomedical applications.

MOHAMED EL ATRASH (Student Member, IEEE) received the B.Sc. degree (Hons.) in electrical engineering from the Electrical Systems Engineering Department, October University for Modern Sciences and Arts (MSA), Cairo, Egypt, in 2011, the M.Sc. degree (Hons.) in wireless mobile communications systems engineering from the University of Greenwich (UoG), U.K., in 2014, and the Ph.D. degree in electrical engineering from Ain Shams University, Cairo, in 2020. His research interests include flexible wearable antennas, high gain, thin, low profile antennas, and EBG/AMC design. Out of his research, he published articles in the IEEE TRANSACTIONS ON ANTENNAS AND PROPAGATION, *IET Microwaves, Antennas and Propagation*, and the *International Journal of Microwave and Wireless Technologies*, as well as, a number of conference papers. He has been a Reviewer of the *IET Microwaves, Antennas and Propagation*, since 2019, where he has reviewed more than 15 journals. He also reviewed for *Microwave and Optical Technology Letters*, *AEU-International Journal of Electronics and Communications*, and *International Journal of RF and Microwave Computer-Aided Engineering*.

● ● ●